Resonant reflectivity from a Ni(110) crystal: Magnetic effects at the Ni 2*p* edges using linearly and circularly polarized photons

Maurizio Sacchi
Laboratoire pour l'Utilisation du Rayonnement Electromagnétique (LURE), Bâtiment 209d, Centre Universitaire Paris-Sud, 91405 Orsay, France

Alessandro Mirone
Institut d' Optique Théorique et Appliquée (IOTA), URA 14 CNRS, BP 147, 91493 Orsay, France
(Received 22 September 1997)

We have measured the magnetization dependence of the resonant reflectivity at the 2*p* edges of Ni in a Ni(110) single crystal. Experiments were performed using both circularly and linearly polarized photons. Large magnetic effects on the reflectivity were observed in both experimental configurations over a wide angular range. A simple model, using the absorption of elliptically polarized light as input, gives results in very good agreement with our data as a whole. We also show that angular- and energy-dependent reflectivity at resonance enhances fine spectroscopic signatures and increases the experimental information concerning the ground state properties of magnetic materials. [S0163-1829(98)05013-9]

I. INTRODUCTION

Resonant magnetic scattering of polarized x rays is a fairly new technique that is rapidly expanding and diversifying both in its applications and experimental approaches.[1] First experiments were performed in the hard x-ray range[2] measuring the Bragg diffraction from crystalline samples containing magnetic elements. Typical examples are the rare earths (2*p* edges) and the actinides (3*d* edges). Soon after, large magnetic effects in the resonant reflectivity from Fe,[3,4] Co,[5] and Ni (Ref. 6) were observed for soft x rays (2*p* edges). At the price of losing structural information, resonant reflectivity has the advantage over Bragg diffraction of not suffering from constraints on the lattice spacing. The 2*p* edges of 3*d* transition metals give very large magnetic effects in resonant scattering, but the corresponding wavelengths would not allow, for instance, Bragg diffraction from metallic single crystals. Reflectivity also makes it possible to cover a wide set of interesting samples (e.g., amorphous materials) that would not give suitable Bragg peaks. Recently, a few examples of resonant Bragg diffraction studies in the soft x-ray region have been reported, where the samples were magnetic multilayers containing 3*d* transition metals.[7–9]

In this paper we present the results of a series of resonant reflectivity experiments at the Ni 2*p* edges of Ni(110), performed using either elliptical or linear polarization of the x rays. Large magnetic effects have been observed in both experimental conditions, with specific angular and polarization dependence. Resonant reflectivity curves have also been calculated by directly solving Maxwell's equations for a dielectric tensor constructed from the experimental absorption curves.

Finally our data give some new indication about the ground state magnetic properties of Ni. This we will discuss in the last section.

II. EXPERIMENTAL DETAILS

The experiment was carried out at the SA-8 beam line of the SuperACO storage ring in LURE (Orsay), using the unfocused radiation from a bending magnet and a double beryl (1010) crystal monochromator giving a resolution of about 300 meV at the Ni 2*p* edges. Entrance slits were used to select the vertical accepted angle: symmetric with respect to the orbit plane in the ring for linearly polarized photons and below (or above) the plane for elliptically polarized light with positive (or negative) helicity. In the latter case, we set the slits 0.5 mrad below plane, obtaining in the range of the 2*p* edges of Ni a circular polarization rate of about 0.4 after the monochromator. Two adjustable jaws delimited the horizontal size of the beam at the sample position in order to keep it about half the size of the projected sample surface.

The reflectivity measurements were performed in the ultrahigh-vacuum chamber already described in Ref. 10, and following the same cleaning procedures for the sample. The Ni(110) crystal was mounted on a soft iron horseshoe magnet with the field applied along the [111] direction in the (110) plane. The crystal-magnet ensemble could be mounted with the [111] direction either parallel or perpendicular to the scattering plane, the former solution being used for the circular polarization experiments, the latter for the linear polarization ones.

Low-angle reflectivity was measured using a linear diode array (each diode integrating over 0.1°) covering the 0°–5° range in θ (grazing angle). The reflectivity around $2\theta=45°$ was monitored using a series of microchannel plates and a resistive anode,[11] forming a low-noise two-dimensional position-sensitive detector. The signal from the resistive anode was integrated over an area corresponding to 0.3°. We tried to determine absolute values of the reflectivity at different angles by comparing the signal on an I_0 monitor (0.8 mm Al foil) with the reading of the diode receiving the direct beam in the absence of the sample, and then keeping the I_0

monitor as a reference for the absolute incoming flux. This procedure does not allow a precise determination of absolute values, but we obtained a set of data (from 0.5 reflectivity at 1° to $1-2\times10^{-5}$ at 22.5°) consistent with a mean surface roughness of about 4 Å for the Ni crystal.

In order to minimize spurious effects on the dichroism, the magnetization of the sample was reversed at each energy point by a 2 A current pulse in the electromagnet. Measurements were usually performed under remanence conditions.

Together with reflectivity, i.e., using the same incoming photon, we also measured the total electron yield (TEY) from the sample. With adequate precautions,[10,12] the TEY provides information concerning the absorption spectrum.

III. CALCULATION OF THE REFLECTIVITY

In order to simulate the reflectivity curves for magnetic Ni, we first built the dielectric tensor starting from experimental absorption curves measured for parallel and antiparallel alignments of photon helicity and sample magnetization. The imaginary part $k^{\pm}$ of the helicity-dependent refractive index $n^{\pm}$ can be obtained directly from the absorption coefficient ($k=\mu\lambda/4\pi$), while the real part $n^{\pm}$ was obtained from the Kramers-Kronig transformation of $k^{\pm}$. Having defined $\epsilon^{\pm}$ as $(n^{\pm})^2$ and assuming that Ni does not exhibit any linear dichroism (Ni has cubic structure and no magnetic linear dichroism has been observed experimentally[13]), the dielectric tensor $\boldsymbol{\epsilon}$ has the following elements:

$$\epsilon_{y'z'}=-\epsilon_{z'y'}=-\frac{i}{2}(\epsilon^{+}-\epsilon^{-}),$$

$$\epsilon_{x'x'}=\epsilon_{y'y'}=\epsilon_{z'z'}=\tfrac{1}{2}(\epsilon^{+}+\epsilon^{-}),$$

$$\epsilon_{x'z'}=\epsilon_{z'x'}=\epsilon_{x'y'}=\epsilon_{y'x'}=0,$$

where x' identifies the magnetization axis. To obtain the reflectivity at the vacuum/nickel interface we solve Maxwell's equations in the form

$$\det\left|k_0^2\boldsymbol{\epsilon}-(k_x^2+k_z^2)I+\begin{pmatrix}k_x^2 & 0 & k_xk_z\\ 0 & 0 & 0\\ k_xk_z & 0 & k_z^2\end{pmatrix}\right|=0, \quad (1)$$

where the coordinate system is defined by x, the intersection between sample surface and scattering plane, y, normal to the scattering plane, and z, normal to the sample surface. In Eq. (1), I is the identity matrix, $\boldsymbol{\epsilon}$ the dielectric tensor defined above written in the (xyz) coordinate system, θ is the grazing angle, $k_x(=k_0\cos\theta)$ and k_z are the x and z components of the wave vector in nickel, and k_0 is the modulus of the wave vector in a vacuum. Equation (1) gives a polynomial of fourth degree in k_z, whose four roots can be split into two couples of solutions according to the sign of the real part of k_z: positive for the two waves propagating in the negative z direction (into the nickel), negative for the two along the positive z direction (towards vacuum). The electromagnetic field in the Ni is written as a linear combination of the four waves with coefficients determined by imposing at the Ni/vacuum interface the condition of continuity of the components of E and B parallel to the interface. Finally, the reflectivity is obtained by imposing the condition of outgoing waves in the substrate.

This description refers to the case of a semi-infinite solid, a model that applies to the reflectivity from a thick Ni crystal. The same method has been developed and integrated in a computer code for a general stacking of (magnetic) layers of finite thickness along the z direction.

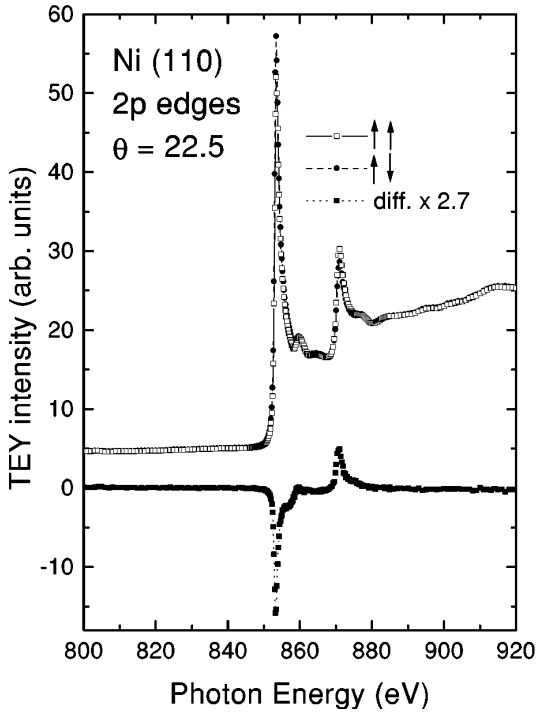

FIG. 1. Ni 2p absorption curves measured in the TEY mode using elliptically polarized photons of negative helicity incident at 22.5° with respect to the [111] magnetization axis. Open squares and solid circles refer to opposite magnetization directions. The difference curve has been multiplied by a factor of 2.7 to correct for the incomplete polarization of the light (degree of circular polarization of 0.4) and for the angle of incidence.

IV. RESULTS AND DISCUSSION

A. Refractive index at the 2p edges of Ni

Figure 1 shows the raw absorption spectra measured at the Ni 2p edges with elliptically polarized photons impinging at 22.5° with respect to the [111] magnetization direction of the sample. In this geometry, saturation effects were considered negligible (less than 3% change in intensity at the $L3$ maximum between $\theta=22.5°$ and 90°). The x-ray magnetic circular dichroism (XMCD) spectrum (difference between magnetization parallel and antiparallel to helicity) is also reported. After correcting for the polarization rate of the light and for the misalignment between magnetization and photon propagation directions (a factor of 2.7 in the difference), these spectra were scaled to the tabulated values[14] for absorption at 800 and 920 eV and then used to construct the dielectric tensor $\boldsymbol{\epsilon}$ for Ni according to the procedure described in Sec. III. All the calculated reflectivity curves that we will show in the rest of the paper have been obtained starting from these absorption data. The real part n of the

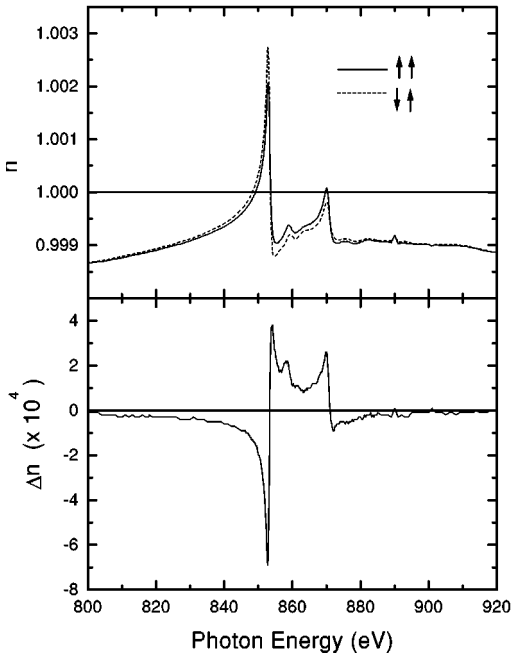

FIG. 2. Real part of the refractive index obtained by Kramers-Kronig transformation of the absorption curves (see Sec. IV A) for the two magnetization-helicity orientations. The difference curve is reported in the bottom panel.

complex refractive index across the Ni $2p$ edges as obtained from the Kramers-Kronig transformation is shown in Fig. 2 for parallel and antiparallel orientations of helicity and magnetization. As mentioned in Sec. II, TEY spectra were always collected together with reflectivity, but due to the very grazing geometry, they are very difficult to exploit in order to construct the dielectric tensor, since they are affected by strong saturation[10,12] and by the reflectivity itself.[15] To verify our procedure for building the dielectric tensor, we also started from another set of TEY spectra collected at $\theta = 10°$. In this case the saturation was large enough (about 15% at the L_3 maximum) to require corrections, but the final results agreed with the data reported in Figs. 1 and 2.

B. Reflectivity of elliptically polarized light

A comparison between experimental and calculated reflectivity of elliptically polarized photons is given in Fig. 3 for a scattering angle 2θ of 4.6°. For these measurements the geometry is such that the magnetization ([111] direction in the crystal surface) and the longer axis of the ellipse described by the electric vector of the light are both within the scattering plane. The magnetization averaged experimental curve in Fig. 3(a) has been scaled to exactly match the calculation and the same multiplying factor has been applied to the difference curve in Fig. 3(b). The asymmetry ratio (difference divided by the sum) reported in Fig. 3(c) is obtained directly from raw data after subtracting the dark current of the diode. This operation is rather delicate for determining the asymmetry ratio close to the minimum of the reflectivity curve. Figure 4 shows that, to the best of our corrections for the dark current, we systematically obtain at the reflectivity minimum a smaller asymmetry ratio than calculated. It is not clear to us at present whether to ascribe this discrepancy to experiment or to calculations.

Nevertheless we want to stress that the agreement is rather good over the explored angular range, especially considering that no free parameter is introduced either in the calculation or in deriving the experimental values of the asymmetry ratio.

C. Reflectivity of linearly polarized light

We also measured the resonant reflectivity of linearly polarized light, with the electric vector in the scattering plane

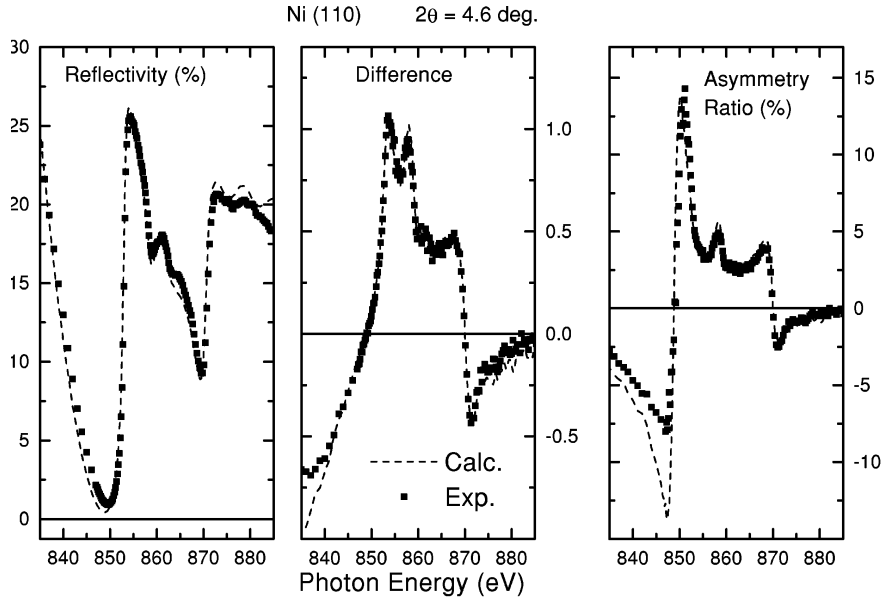

FIG. 3. Reflectivity of elliptically polarized photons from the Ni(110) crystal for a scattering angle 2θ of 4.6°. The left panel shows the magnetization-averaged percent reflectivity and the central panel its variation with the magnetic field direction. The right panel reports the asymmetry ratio (in percent) defined as the difference divided by the sum. Squares are experimental data and dashed lines are calculations (see Sec. III).

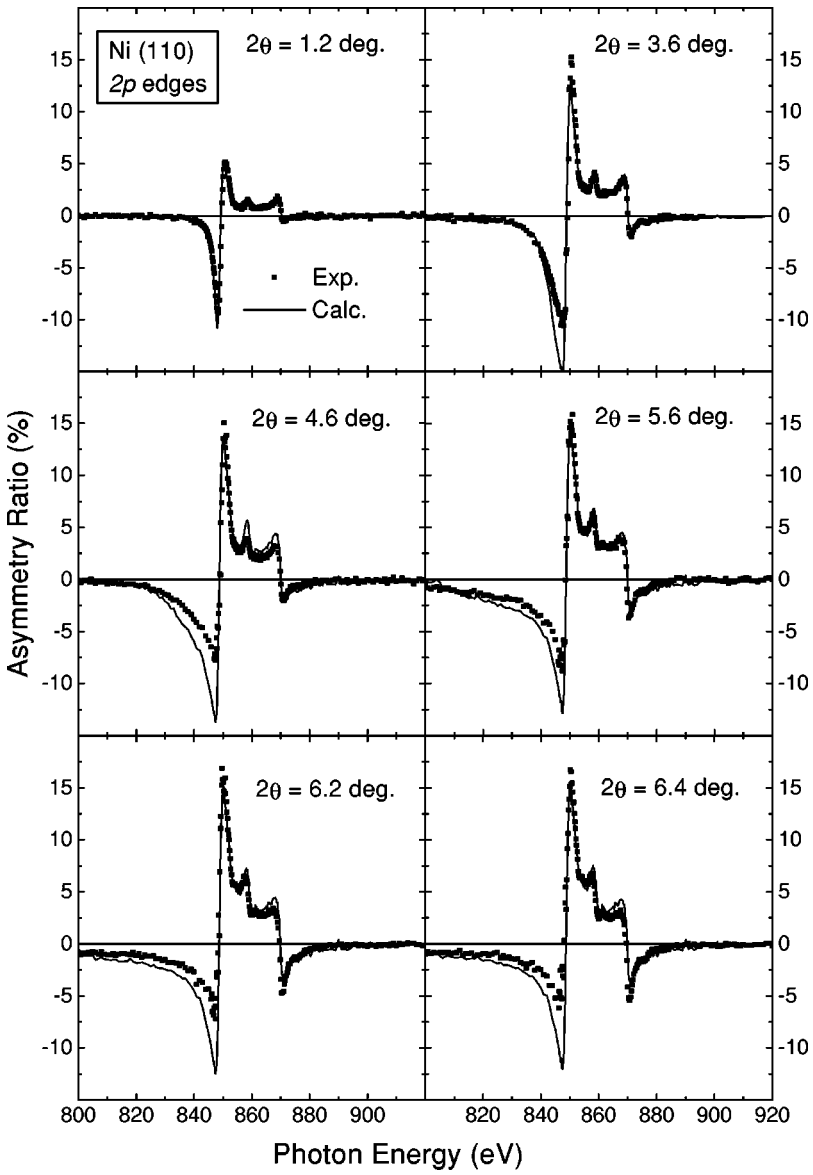

FIG. 4. Experimental (squares) and calculated (lines) asymmetry ratio curves for elliptically polarized light and different scattering angles.

(p polarization) and the magnetization of the sample orthogonal to it. This experimental geometry (characterized by the three vectors of polarization in, polarization out, and magnetization) has a defined handedness (left or right) that depends on the sign of the magnetization (up or down). Considering the resonant contribution to the scattering amplitude and following the formalism of Hannon *et al.*,[16] the asymmetry ratio in this configuration is given by

$$\frac{I^{\uparrow}-I^{\downarrow}}{I^{\uparrow}+I^{\downarrow}}=\frac{\mathrm{Im}\{\alpha\}\sin(4\theta)}{1+\mathrm{Re}\{\alpha\}\cos(4\theta)}, \tag{2}$$

where α contains the oscillator strengths giving the absorption of circularly polarized photons as a function of their helicity (see also Refs. 17 and 18). The relation between dichroism in the reflectivity of p-polarized light and in the absorption of circularly polarized light is then well established.

Figure 5 shows the asymmetry ratio curves obtained at two different scattering angles, together with the corresponding calculations. As for circular polarization, the agreement is rather good, even if now the experimental input for the model calculation has been obtained in a completely different geometry and, in particular, using photons of a different polarization state.

From Eq. (2), the dichroism is expected to increase with the scattering angle and change sign when passing through $2\theta=90°$, where it has to go to zero.[17] The reflectivity and asymmetry ratio obtained for $2\theta=45°$ are shown in Fig. 6: Even if affected by the small signal-to-noise ratio, our results agree fairly well with the corresponding calculations. Fitting our data using Eq. (2) over the available angular range and leaving α (complex) as a free parameter, we could predict a maximum in the magnetic signal for 2θ values around 70°–80° degrees. Unfortunately, these scattering angles imply a further reduction of about two orders of magnitude in the reflectivity, making the measurement unrealistic with our ex-

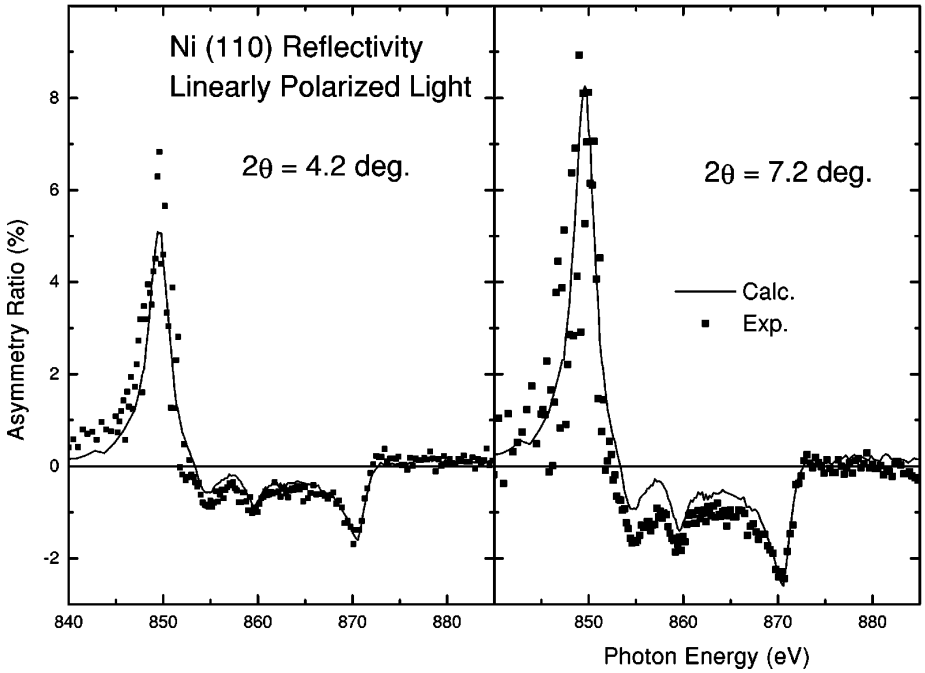

FIG. 5. Experimental (squares) and calculated (lines) asymmetry ratio curves for linearly polarized light and different scattering angles.

perimental setup. Nonetheless, resonant magnetic reflectivity using p-polarized light at high scattering angles represents, in our view, an important tool for a semiquantitave element-selective magnetometry if one disposes of high-intensity synchrotron sources, since it can give very high relative magnetic effects. Figure 7 compares the results of three different measurements, all performed at $\theta=22.5°$: absorption (TEY) and reflectivity of elliptically polarized photons (0.4 circular polarization rate), and reflectivity of linearly p-polarized photons. For each measurement, two spectra were collected, reversing the magnetization along the [111] axis of the Ni crystal. The sums are reported in the left panel (they are all normalized between 0 and 100) and the difference spectra appear in the right panel. The difference in the absorption remains much smaller than in reflectivity even when normalized to a rate of 100% circular polarization. The difference curves for the two reflectivity experiments are of comparable magnitude after polarization correction.

D. Abundance of structure in resonant reflectivity spectra

In this last section we will discuss, using Ni as an example, how dichroism in reflectivity can help us understand

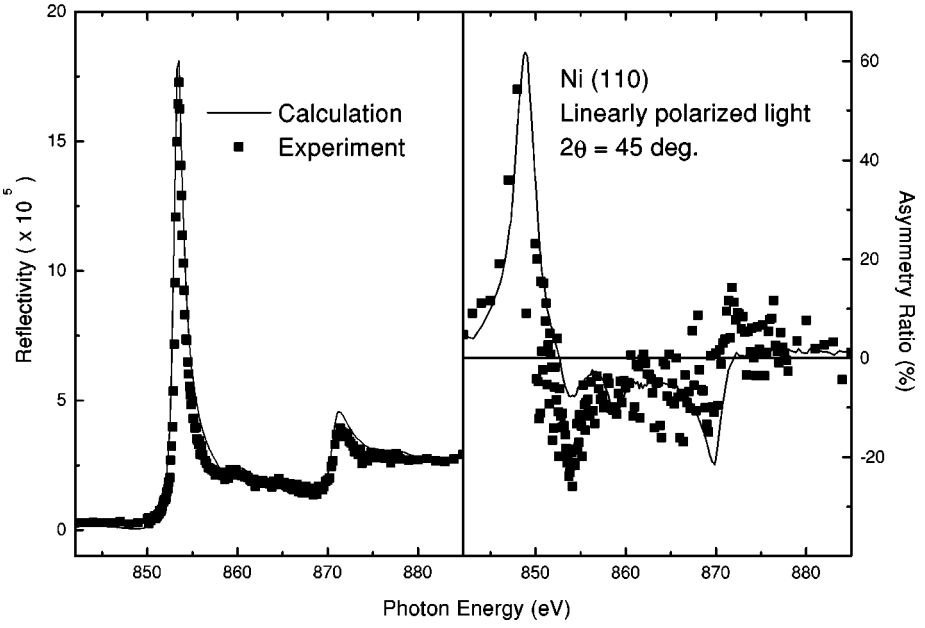

FIG. 6. Magnetization-averaged reflectivity (left) and asymmetry ratio (right) for linearly polarized light and $2\theta=45°$. Squares are experimental data, and lines are calculations.

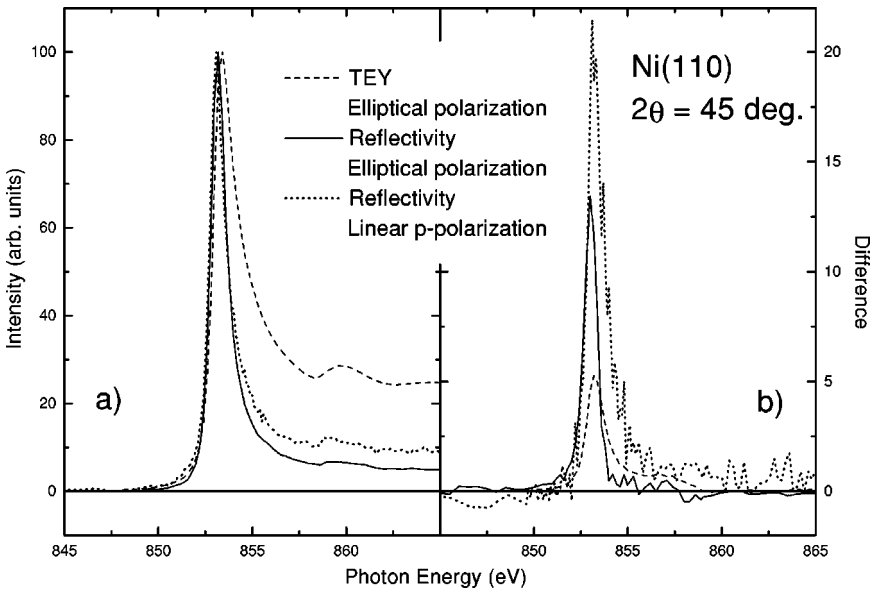

FIG. 7. Comparison between the TEY and reflectivity measured with elliptically polarized light and reflectivity for linearly polarized light around the Ni $2p$ edges (left panel). All curves are obtained for an angle of incidence $\theta=22.5°$ and normalized to the same peak intensity. The right panel compares the corresponding difference curves obtained upon reversal of the magnetization along the [111] direction of the Ni crystal.

the electronic and magnetic properties of materials and refine parametrized model calculations.

The absorption and circular dichroism spectra at the $2p$ edges of metallic Ni have been extensively discussed in the past.[19–25] Following the notation introduced in Ref. 20, the $2p_{3/2}$ absorption presents a main peak (located at 853.4 eV in our case; see Fig. 1) followed by a weaker satellite A about 6.3 eV higher in energy. The main feature of the XMCD spectrum more or less coincides in energy with the absorption peak (853.3 eV) while the satellite B in the dichroism is about 4 eV higher in energy and no magnetization dependence is observed in correspondence to satellite A.[10,20] These experimental results have been discussed both in terms of a one electron approach[21,24] and according to the Anderson impurity model with configuration interaction.[22,23] The latter was capable of explaining the experimental results by defining the ground state of metallic nickel as an admixture of $3d^8$, $3d^9\upsilon$ and $3d^{10}\upsilon^2$ configurations. Jo and Sawatzky[22] and van der Laan and Thole[23] obtained different relative weights of the d^9 and d^{10} contributions in their calculations. In Ref. 22 a value of 65% for $3d^9$ was determined by comparison with the experimental $2p$ absorption data.[20] In Ref. 23, the best agreement with the results of an ensemble of $2p$ and $3p$ absorption and photoemission experiments was found using a $3d^9$ weight of 49%. Moreover, van der Laan and Thole indicated in their work that a non-negligible magnetic signal should appear in correspondence to satellite A, a feature that was not observed experimentally.[10,20]

We believe that resonant reflectivity at the $2p$ edges of Ni can supply further experimental information as far as the detailed modeling of the Ni ground state is concerned. The presence of interference terms containing an angular dependence makes the reflected intensity a very sensitive probe of the constituting transitions forming the $2p$ edges. Figure 8 shows the angular dependence of the XMCD curves in reflectivity for elliptically polarized photons. The curves are normalized on an arbitrary scale in order to better compare the line shapes. One can note in Fig. 8 the existence of a sort of optimized angular range over which specific structures are emphasized. For instance, structure B of XMCD spectra in absorption is usually no more than a shoulder to the main peak, but in reflectivity and for grazing angles around 2° it can represent the strongest and sharpest peak of the dichro-

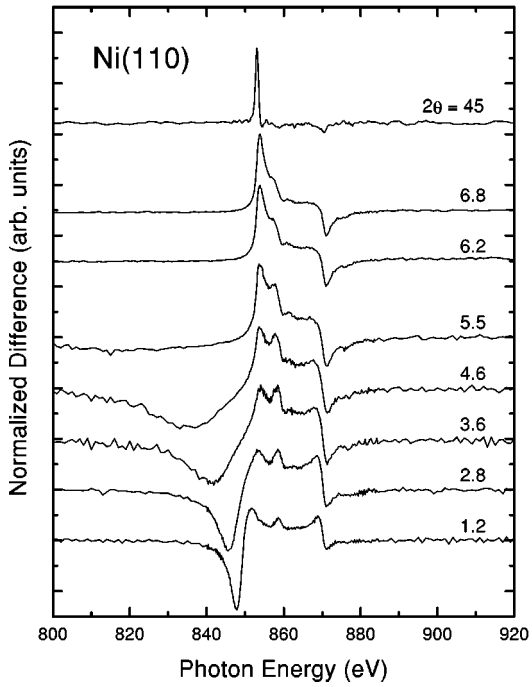

FIG. 8. Magnetic part of the reflectivity of elliptically polarized photons from the Ni(110) crystal as a function of the scattering angle 2θ. The curves are arbitrarily scaled for a better comparison.

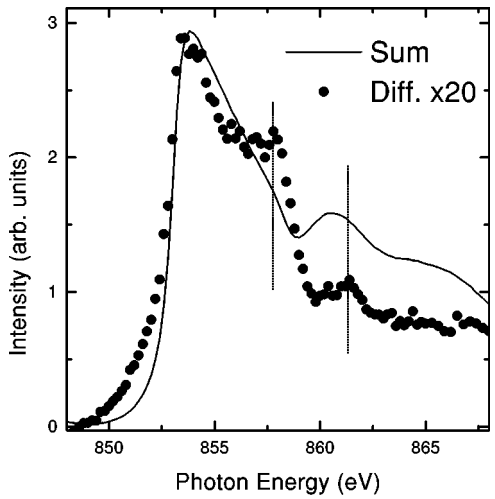

FIG. 9. Sum and difference of the $2\theta=5.5°$ reflectivity curves for opposite magnetization directions along the [111] axis. The energy range corresponds to the L_3 ($2p_{3/2}$) edge of Ni. Vertical dotted lines help to locate the magnetic satellites on the magnetization-averaged spectrum.

ism spectrum. On the other hand, the analysis of the magnetic effects in the pre-edge region (840–850 eV) which are related to the magnetic part of n (see Fig. 2) can take advantage of the angular range below 2°.

This behavior can be qualitatively understood remembering that, given a certain grazing angle θ, we can define a critical value n_c of the real part of the index of refraction for having total external reflection. Since $n=1$ for vacuum, n_c is always lower than 1 and decreases with θ. Around 2.3°, for instance, n_c is about 0.9992: According to Fig. 2 total external reflection in the region of the L_3 edge of Ni can only occur above 854 eV, i.e., above the absorption maximum. Hence at this angle the reflectivity will be relatively suppressed below 854 eV and enhanced between 854 and 860 eV. The same qualitative argument holds for explaining the enhanced magnetic effects in the satellites energy region over a certain angular range.

Between 2° and 3° we can indeed observe a slight magnetization dependence in the energy region corresponding to satellite A of the absorption spectrum. Figure 9 compares the reflectivity and the corresponding dichroism curves for $2\theta=5.5°$. Two remarks can be made: (i) At the same energy as satellite B of XMCD spectra a shoulder in the magnetization-averaged reflectivity is observed (see also Fig. 3). In Refs. 21 and 24 the authors stated ''It is provocative that the B feature appears prominently in the MCD spectrum but is imperceptible in the total absorption spectrum.'' Our data show that feature B does not appear in the absorption spectrum because it is too close to the intense main peak, as suggested in Ref. 23, but it can be relatively enhanced in reflectivity by choosing an appropriate angle. (ii) In the energy region of satellite Awe can clearly identify a small peak in the XMCD curve, as predicted by van der Laan and Thole in Ref. 23. It is located on the high-energy side of A (the separation between the maxima is about 1 eV), suggesting that only part of the transitions constituting A contributes to the difference curve, i.e., shows a magnetization dependence.

We believe that these observations, the latter in particular, introduce a new experimental input for model calculations that should motivate further theoretical investigation. It is rather straightforward, once a model has been developed as in Refs. 22 and 23, to calculate reflectivity curves in addition to absorption, and a detailed comparison with experiment would certainly increase the understanding of the ground state properties of nickel.

V. CONCLUSIONS

We have measured the specular reflectivity from a Ni(110) crystal over the photon energy range including the $2p$ edges of Ni. Magnetic effects on the resonant reflectivity have been observed in two different geometries: (i) using elliptically polarized photons and orienting the [111] magnetization axis in the scattering plane and (ii) using linearly polarized photons with the electric vector oriented in the scattering plane and the [111] direction of the crystal orthogonal to it. In both cases a change in the magnetization direction along the [111] axis corresponds to the same symmetry operation, i.e., a reflection with respect to the (111) plane.

The ensemble of the experimental results was reproduced within a simple model based on the solution of Maxwell's equations for a plane wave propagating in a dichroic medium. To construct the dielectric tensor for Ni we started out using experimental polarization-dependent absorption curves measured with elliptically polarized light. The calculations reproduce, with very good accuracy, the magnetic dichroism in the reflectivity of both elliptically and linearly polarized light.

The magnetic reflectivity of linearly p-polarized light shows a strong angular dependence of the magnetic asymmetry ratio, which can be much higher than in circular polarization absorption experiments. At the price of a reduced signal intensity, we are able to obtain, in this configuration, a much better magnetic contrast, while maintaining element selectivity as in absorption spectroscopy. It is also worth remembering that the standard polarization state of x rays from a storage ring is linear polarization, and hence it is easier to obtain.

Our results clearly show also the richness of resonant reflectivity spectra, as pointed out in Sec. IV D. In terms of fundamental properties, reflectivity spectra do not contain much more independent information than (polarization-dependent) absorption. Still it is obvious from the previous presentation that the ensemble of the reflectivity spectra (angle, polarization, and energy dependent) contains an amount of structure that allows a deeper and finer discussion of the fundamental properties and a certainly more reliable refinement of parametrized models. Maybe the *abundance of structure* is not a well-defined concept, but Figs. 8 and 9 are a good example of what we mean.

To conclude, we want to underline a few relevant technical aspects that we did not take advantage of in this work, but which contribute to make resonant reflectivity an interesting tool for magnetic studies. It is element selective, since we work at the resonance of a specific element, just as in absorption. It is a photon-in–photon-out process, and hence not affected by the presence of external magnetic fields, not

even strong and/or time-dependent fields (thus, for instance, element-specific hysteresis curves may be drawn[6,26]). It has the necessary sensitivity for studying coverages of less than one atomic layer on a clean surface,[26] yet its field of view extends well below the surface, allowing us to investigate buried layers also. Ultrahigh vacuum is not required, and the analysis can be performed in a controlled atmosphere to study dynamical processes (deposition, corrosion, etc.).

Overall, these characteristics make resonant reflectivity an important tool for both fundamental and applied research on magnetic materials and a technique that in many aspects complements others in the field of magnetic dichroism.

ACKNOWLEDGMENTS

We thank Coryn Hague and Jean-Michel Mariot (Laboratoire de Chimie-Physique, Paris) for interesting and useful discussions, for their critical reading of the manuscript, and for lending us their position-sensitive detector.

[1] See, e.g., D. B. McWhan, J. Synchrotron Radiat. **1**, 83 (1994), and references therein.

[2] D. Gibbs, D. R. Harshman, E. D. Isaacs, D. B. McWhan, D. Mills, and C. Vettier, Phys. Rev. Lett. **61**, 1241 (1988); E. D. Isaacs, D. B. McWhan, C. Peters, G. E. Ice, D. P. Siddons, J. B. Hastings, Ch. Vettier, and O. Vogt, *ibid.*, **62**, 1671 (1989).

[3] C.-C. Kao, J. B. Hastings, E. D. Johnson, D. P. Siddons, and G. C. Smith, Phys. Rev. Lett. **65**, 373 (1990).

[4] V. Chakarian, Y. U. Idzerda, C.-C. Kao, and C. T. Chen, J. Magn. Magn. Mater. **165**, 52 (1997).

[5] C.-C. Kao, C. T. Chen, E. D. Johnson, J. B. Hastings, H. J. Lin, G. H. Ho, G. Meigs, J-M. Brot, S. L. Hulbert, Y. U. Idzerda, and Ch. Vettier, Phys. Rev. B **50**, 9599 (1994).

[6] M. Sacchi, J. Vogel, and S. Iacobucci, J. Magn. Magn. Mater. **147**, L11 (1995).

[7] J-M. Tonnerre, L. Sève, D. Raoux, G. Soullié, B. Rodmacq, and P. Wolfers, Phys. Rev. Lett. **75**, 740 (1995).

[8] C. F. Hague, J.-J. Gallet, J.-M. Mariot, and M. Sacchi, in *Raman Emission by X-rays*, edited by D. Ederer and J. McGuire (World Scientific, Singapore, 1996), p. 137.

[9] M. Sacchi, C. F. Hague, E. M. Gullikson, and J. H. Underwood, Phys. Rev. B **57**, 108 (1998).

[10] J. Vogel and M. Sacchi, Phys. Rev. B **49**, 3230 (1994).

[11] C. F. Hague, J.-M. Mariot, G. Y. Guo, K. Hricovini, and G. Krill, Phys. Rev. B **51**, 1370 (1995).

[12] J. Vogel and M. Sacchi, J. Electron Spectrosc. Relat. Phenom. **67**, 181 (1994); W. L. O'Brien and B. P. Tonner, Phys. Rev. B **50**, 12 672 (1994).

[13] We have tested this point by measuring the $2p$ edges of metallic Ni layers in transmission mode: To better than 10^{-4} (limited by noise and instabilities) we did not observe any magnetic effect on the absorption of linearly polarized photons [F. C. Vicentin, S. Turchini, F. Yubero, J. Vogel, and M. Sacchi (unpublished)].

[14] B. L. Henke, E. M. Gullikson, and J. C. Davis, At. Data Nucl. Data Tables **54**, 181 (1993).

[15] D. Alders, T. Hibma, G. A. Sawatzky, K. C. Cheung, G. E. van Dorssen, M. D. Roper, H. A. Padmore, G. van der Laan, J. Vogel, and M. Sacchi, J. Appl. Phys. **82**, 3120 (1997).

[16] J. P. Hannon, G. T. Trammell, M. Blume, and D. Gibbs, Phys. Rev. Lett. **61**, 1245 (1988).

[17] P. Carra, M. Altarelli, and F. de Bergevin, Phys. Rev. B **40**, 7324 (1989); P. Carra and M. Altarelli, Phys. Rev. Lett. **64**, 1286 (1990).

[18] C. Tang, W. G. Stirling, G. H. Lander, D. Gibbs, W. Herzog, P. Carra, B. T. Thole, K. Mattenberger, and O. Vogt, Phys. Rev. B **46**, 5287 (1992).

[19] L. C. Davis, J. Appl. Phys. **59**, R25 (1986), and references therein.

[20] C. T. Chen, F. Sette, Y. Ma, and S. Modesti, Phys. Rev. B **42**, 7262 (1990).

[21] C. T. Chen, N. V. Smith, and F. Sette, Phys. Rev. B **43**, 6785 (1991).

[22] T. Jo and G. A. Sawatzky, Phys. Rev. B **43**, 8771 (1991).

[23] G. van der Laan and B. T. Thole, J. Phys. Condens. Matter **4**, 4181 (1992).

[24] N. V. Smith, C. T. Chen, F. Sette, and L. F. Mattheiss, Phys. Rev. B **46**, 1023 (1992).

[25] N. Mainkar, D. A. Browne, and J. Callaway, Phys. Rev. B **53**, 3692 (1996).

[26] M. Sacchi, Surf. Rev. Lett. **4**, 343 (1997).